Electronic Supplementary Material (ESI) for Journal of Materials Chemistry C.

Supporting Information

Enhanced strains by flexible nanoscale domain structure in BNKT-SBT relaxor ferroelectrics

Xiaoyuan Sun, Hao Qian, Tianyang Zheng, Fujun Chen, Yunfei Liu*, Yinong Lyu*

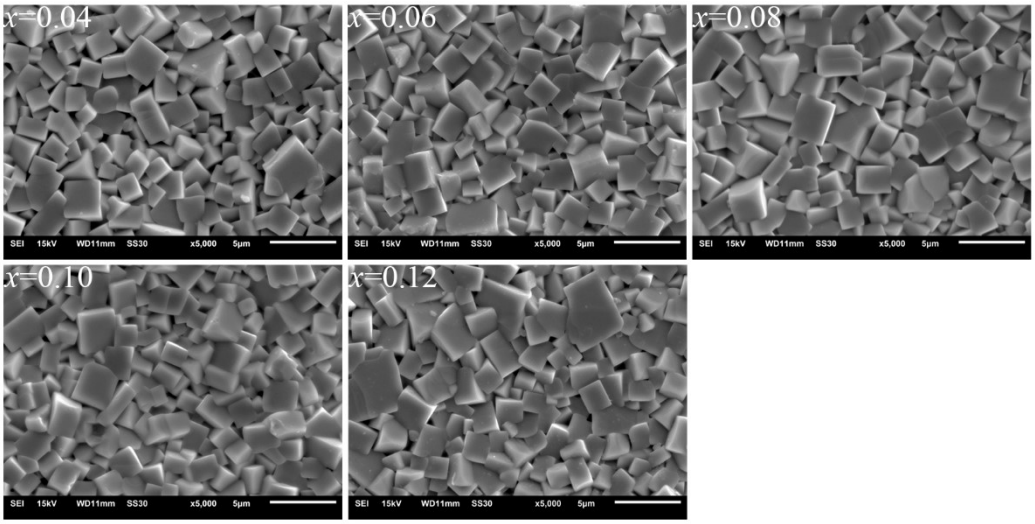

Fig. S1 SEM images of BNKT-100*x*SBT ceramics.

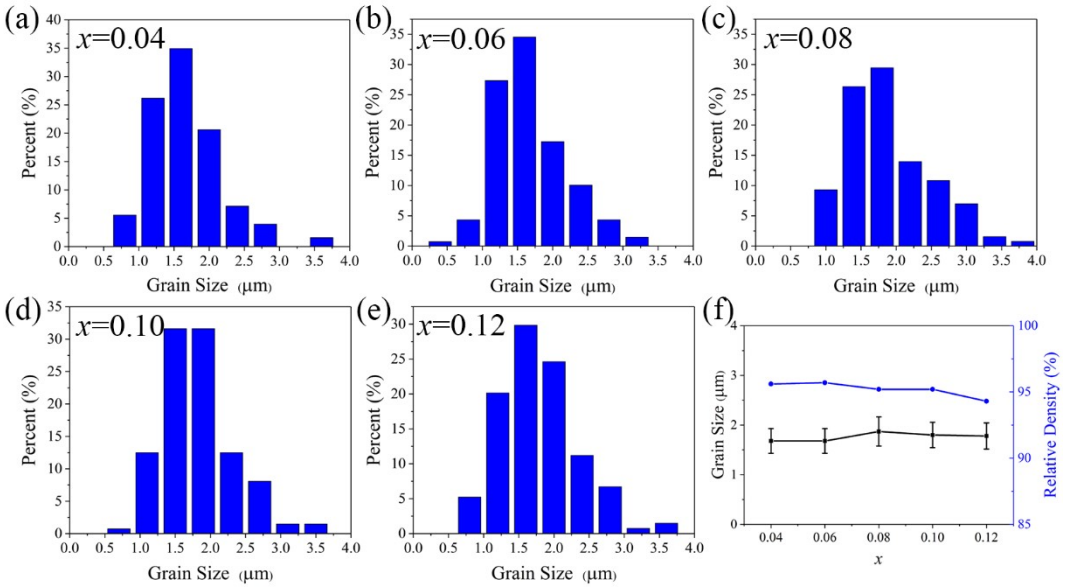

Fig. S2 Grain size distribution diagrams of BNKT-100*x*SBT ceramics derived from SEM images, (a) *x*=0.04, (b) *x*=0.06, (c) *x*=0.08, (d) *x*=0.10, (e) *x*=0.12 and (f) average grain size as a function of *x* and relative density measured by the Archimedes method.

Fig. S1 shows the surface morphology obtained on the sintered ceramics surface without thermally etched by SEM. The grain is relatively uniform and grain boundaries are clear, showing regular grains close to a cube. Fig. S2 shows the grain size derived from SEM images using Nano Measurer software with an average size of 1.5-2 μm. Thus, the effect of grain size on properties is limited because of the almost equivalent grain size. All ceramics are relatively dense, and the relative densities tested by the Archimedes method are all above 94%.

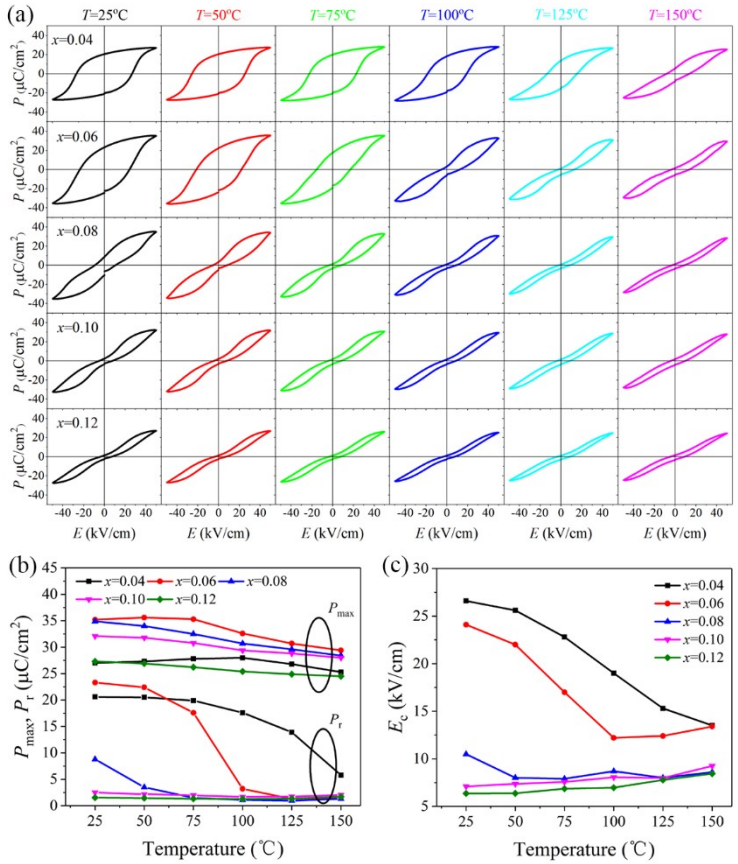

Fig. S3 (a) Temperature-dependent *P*-*E* loops of BNKT-100*x*SBT ceramics. Variation of P_{max}, P_r (b) and E_c (c).

Fig. S3 shows that the hysteresis loops of all samples appear pinched with the increase of the temperature, indicating that the temperature-induced nonergodic-ergodic relaxor phase transition occurred. The reduced residual polarization (P_r) and coercive field (E_c) are ascribed to the increased ergodicity. When $x \leq 0.08$, P_r and E_c decrease obviously with increasing temperature. But P_r and E_c stay roughly the same when $x \geq 0.10$ which is attributed to the weak temperature-induced nonergodic-ergodic phase transition due to greatly decreased nonergodic phase. For BNKT-4SBT ceramics, P_r almost has no

decrease from 25 to 75 ℃. However, P_r decreases significantly at 100 ℃. For BNKT-6SBT ceramics, P_r has decreased obviously at 75 ℃. For BNKT-8SBT ceramics, a significant decrease in P_r occurs at 50 ℃. These temperatures are consistent with the T_{F-R} shown in the temperature-dependent dielectric constants. Moreover, the P_{max} of BNKT-SBT ceramics does not decrease significantly when the temperature increases, showing that the polarization performance is relatively stable even at 150 ℃. Referring to previous studies (see Table S1), the good thermal stability in P_{max} may reflect the good thermal stability of strain properties to a certain extent. The thermal stability of some reported BNT-based ceramics, KNN-based ceramics and BT-based ceramics were compared and summarized in Table S1.

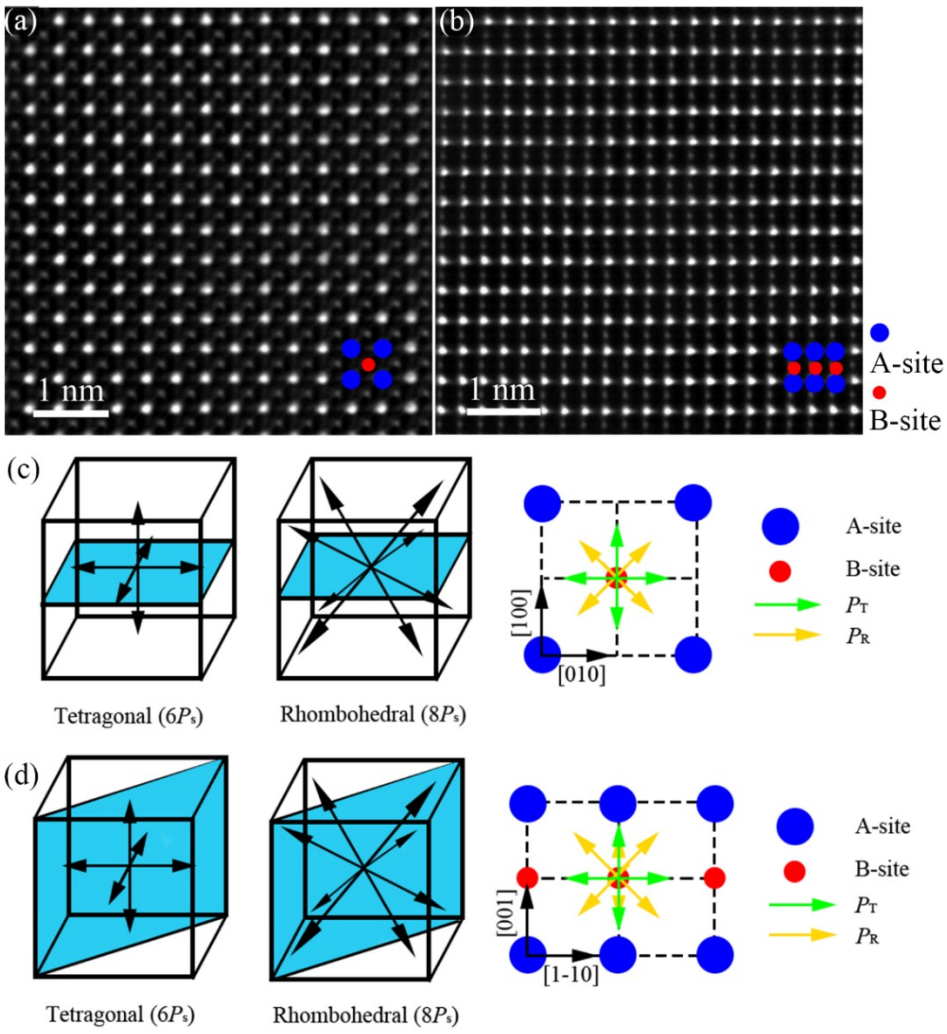

Fig. S4 Atomic-resolution STEM HAADF images of BNKT-8SBT ceramics along [001] zone axis (a) and along [110] zone axis (b) with the positions of A, B-site atomic columns marked accordingly. The schematic directions of spontaneous

polarization (P_s) for R, T phases and projection along the [001] zone axis (c) and along [110] zone axis (d).

Fig. S4 (a) and (b) show the atomic-resolution STEM HAADF images obtained along the [001] and along [110]. Due to the Z-contrast feature of HAADF images, the A-site and B-site atomic columns can be clearly distinguished by obvious intensity differences. The positions of the A and B-site atomic columns are marked in Fig. S4 (a) and (b). According to the atomic position by 2D Gaussian fitting, the displacement of Ti^{4+} columns (B sites) off the ideal cubic position set by the mass center of the four neighboring A-site columns is calculated. The atomic displacement is expressed as a vector from the center of four nearest A-site neighbors to the center of Ti^{4+}. The direction and length of the arrows present the orientation and magnitude of the displacement. For pure T and R phases, the permitted directions of P_s vectors is <100> and <111>, respectively, as schematically shown in Fig. S4 (c) and (b). And the schematic projections along [001] zone axis and along [110] zone axis are marked accordingly.

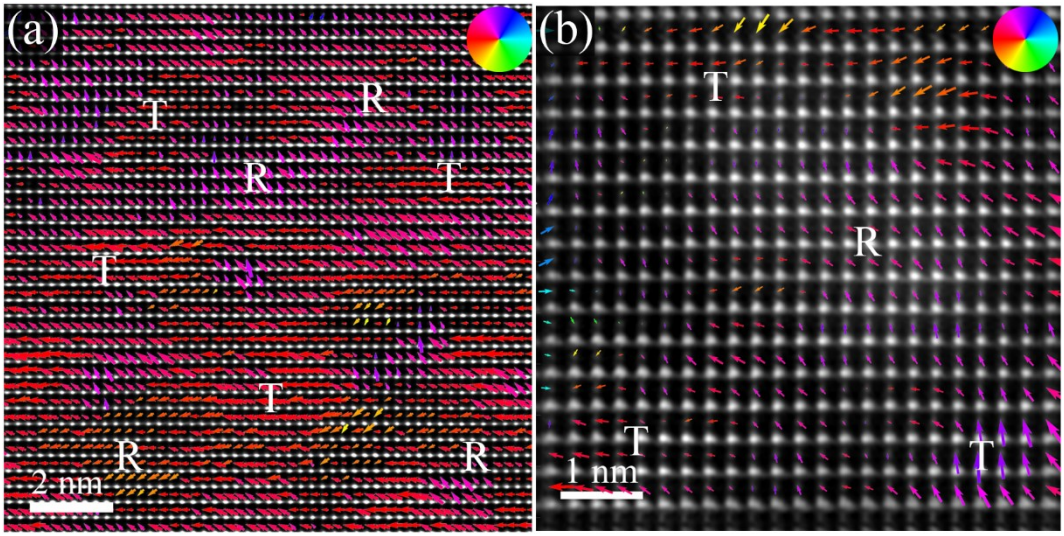

Fig. S5 Atomic-resolution STEM HAADF images of BNKT-8SBT ceramics along [110], with the displacement vector map overlaid on it. The colors indicate the orientation of the displacement vector. (a) HAADF image characterized on a bigger scale, illustrating the coexistence of R and T nanoscale domains. (b) HAADF image characterized on a smaller scale, showing a continuous displacement rotation between R and T nanodomains.

Table S1 Thermal stabilities of some reported lead-free ceramics

Materials	Temperature Range (ºC)	P_{max} Fluctuation (%)	S_{max} Fluctuation (%)	Ref.
BNKT-NN	30-120	25	24.7	[1]
BNKLiTN–ST	25-150	29.7	32.3	[2]
BNT-BT-SL	30-110	18.9	23	[3]
BNT-100*x*Li	30-90	15	13.4	[4]
KNNS–BNKH	27-140	26.7	27	[5]
KNNT-BNKZ-SZ	25-200	18	17.5	[6]
0.5Mn:KNN-T	25-150	13	11	[7]
BTS-BCT	10-50	19.4	15.8	[8]
BZT	30-120	35	40.9	[9]
BNKT-8SBT	25-150	17.6	-	This work

References

1 G. Dong, H. Fan, J. Shi and M. Li, *J. Am. Ceram. Soc.*, 2015, **98**, 1150-1155.

2 R. A. Malik, A. Hussain and A. Maqbool, *J. Am. Ceram. Soc.*, 2015, **98**, 3842-3848.

3 N. Zhao, H. Fan, J. Ma, X. Ren, Y. Shi and Y. Zhou, *Ceram. Int.*, 2018, **44**, 11331-11339.

4 S. Gao, Z. Yao, L. Ning, G. Dong, H. Fan and Q. Li, *Adv. Eng. Mater.*, 2017, **19**, 1700125.

5 T. Zheng, H. Wu, Y. Yuan, X. Lv, Q. Li, T. Men, C. Zhao, D. Xiao, J. Wu, K. Wang, J. Li, Y. Gu, J. Zhu and S. J. Pennycook, *Energ. Environ. Sci.*, 2017, **10**, 528-537.

6 W. Feng, Z. Cen, S. Liang, B. Luo, Y. Zhang, Y. Zhen, X. Wang and L. Li, *J. Alloy. Compd.*, 2019, **786**, 498-506.

7 P. Li, X. Chen, F. Wang, B. Shen, J. Zhai, S. Zhang and Z. Zhou, *ACS Appl. Mater. Inter.*, 2018, **10**, 28772-28779.

8 C. Zhao, H. Wu, F. Li, Y. Cai, Y. Zhang, D. Song, J. Wu, X. Lyu, J. Yin, D. Xiao, J. Zhu and S. J. Pennycook, *J. Am. Chem. Soc.*, 2018, **140**, 15252-15260.

9 L. Jin, J. Qiao, L. Wang, L. Hou, R. Jing, J. Pang, L. Zhang, X. Lu, X. Wei, G. Liu and Y. Yan, *J. Alloy. Compd.*, 2019, **784**, 931-938.